The Large Interferometer For Exoplanets (LIFE): A space mission for mid-infrared nulling interferometry

Adrian M. Glauser[a], Sascha P. Quanz[a,b], Jonah Hansen[a], Felix Dannert[a], Michael Ireland[c], Hendrik Linz[d], Olivier Absil[e], Eleonora Alei[f], Daniel Angerhausen[a], Thomas Birbacher[a], Denis Defrère[g], Andrea Fortier[h], Philipp A. Huber[a], Jens Kammerer[i], Romain Laugier[g], Tim Lichtenberg[j], Suvrath Mahadevan[bv], Taro Matsuo[bg], Michael R. Meyer[cc], Lena Noack[k], Mohanakrishna Ranganathan[a], Sarah Rugheimer[l], Vladimir Airapetian[f], Yann Alibert[h], Pedro J. Amado[m], Marius Anger[n], Narsireddy Anugu[o], Max Aragon[p], David J. Armstrong[q], Amedeo Balbi[r], Olga Balsalobre-Ruza[s], Deepayan Banik[t], Mathias Beck[a], Surendra Bhattarai[u], Jonas Biren[v], Jacopo Bottoni[a], Marrick Braam[w], Alexis Brandeker[x], Lars A. Buchhave[y], José A. Caballero[s], Juan Cabrera[z], Ludmila Carone[aa], Óscar Carrión-González[ab], Amadeo Castro-González[s], Kenny Chan[ac], Ligia F. Coelho[ad], Tereza Constantinou[ae], Nicolas Cowan[af], William Danchi[f], Colin Dandumont[ag], Jeanne Davoult[ah], Arjun Dawn[ai], Jean-Pierre P. de Vera[aj], Pieter J. de Visser[ak], Caroline Dorn[a], Juan A. Duque Lara[al], Mark Elowitz[am], Steve Ertel[an,ao], Yuedong Fang[ap], Simon Felix[aq], Jonathan Fortney[ar], Malcolm Fridlund[as,at], Antonio García Muñoz[au], Cedric Gillmann[b], Gregor Golabek[av], John Lee Grenfell[z], Greta Guidi[aw], Octavio Guilera[ax], Janis Hagelberg[ay], Janina Hansen[a], Jacob Haqq-Misra[az], Nathan Hara[ba], Ravit Helled [bb], Konstantin Herbst[bc], Nina Hernitschek[bd], Sasha Hinkley[be], Takahiro Ito[bf], Satoshi Itoh[bg], Stavro Ivanovski[bh], Markus Janson[x], Anders Johansen[bi], Hugh Jones[bj], Stephen Kane[bk], Daniel Kitzmann[ah], Andjelka B. Kovacevic[bl], Stefan Kraus[be], Oliver Krause[d], J. M. Diederik Kruijssen[bm,bn], Rolf Kuiper[bo], Alen Kuriakose[g], Lucas Labadie[bp], Sylvestre Lacour[ab], Antonino F. Lanza[bq], Laurits Leedjärv[br], Monika Lendl[ay], Michaela Leung[bs], Jorge Lillo-Box[s], Jérôme Loicq[bt], Rafael Luque[bu], Liton Majumdar[bw,bx], Fabien Malbet[by], Franco Mallia [bz], Joice Mathew[c], Elisabeth Matthews[d], Victoria Meadows[ca], Bertrand Mennesson[cb], Karan Molaverdikhani[ap], Paul Mollière[d], John Monnier[cc], Ramon Navarro[cd], Benard Nsamba[ce,cf,cg], Kenshiro Oguri [ch], Apurva Oza[cb], Enric Palle[ci], Carina Persson[at], Joe Pitman[cj], Eva Plávalová[ck], Francisco J. Pozuelos[m], Andreas Quirrenbach[cl], Ramses Ramirez[cm], Ansgar Reiners[cn], Ignasi Ribas[co,cp], Malena Rice[cq], Berke Cow Ricketti[cr], Peter Roelfsema[cs], Amedeo Romagnolo[ct], María Paula Ronco[ax], Martin Schlecker[an], Jessica Schonhut-Stasik[cu], Edward Schwieterman[bs], Antranik A. Sefilian[cv], Eugene Serabyn[cb], Chinmay Shahi[cw], Siddhant Sharma[az], Laura Silva[bh], Swapnil Singh[cx], Evan L. Sneed[bk], Locke Spencer[cy], Vito Squicciarini[ab], Johannes Staguhn[cz,f], Karl Stapelfeldt[cb], Keivan Stassun[cu], Motohide Tamura[da], Benjamin Taysum[z], Floris van der Tak[cs,j], Tim A. van Kempen[cs], Gautam Vasisht[cb], Haiyang S. Wang[bi], Robin Wordsworth[db], and Mark Wyatt[ae]

[a]ETH Zurich, Institute for Particle Physics and Astrophysics, 8093 Zurich, Switzerland
[b]ETH Zurich, Department of Earth Sciences, 8092 Zurich, Switzerland
[c]Research School of Astronomy and Astrophysics, Australian National Univ., ACT 2600, AUS
[d]Max-Planck-Institut für Astronomie, Königstuhl 17, 69117 Heidelberg, Germany
[e]STAR Institute, University of Liège, 19C allée du Six Août, 4000 Liege, Belgium
[f]NASA Goddard Space Flight Center, 8800 Greenbelt Road, Greenbelt, MD 20771, USA
[g]Institute of Astronomy, KU Leuven, Celestijnenlaan 200D, 3001 Leuven, Belgium
[h]Center for Space and Habitability, University of Bern, 3012 Bern, Switzerland
[i]European Southern Observatory, Karl-Schwarzschild-Str. 2, 85748 Garching, Germany

[j]Kapteyn Astronomical Institute, University of Groningen, 9700 AV Groningen, NL
[k]Freie Universität Berlin, Department of Earth Sciences, Berlin, Germany
[l]Department of Physics and Astronomy,York University, Toronto, Canada
[m]Instituto de Astrofisica de Andalucía (CSIC). Glorieta de la Astronomia s/n, 18008 Granada
[n]Aalto University, P.O. Box 11000 (Otakaari 1B), FI-00076 AALTO, Finland
[o]The CHARA Array of Georgia State University, Mount Wilson Observatory, CA 91023, USA
[p]Mines Paris PSL Centre Observation, Impacts, Energie - O.I.E., 06560 Valbonne, France
[q]University of Warwick, Gibbet Hill Road, Coventry, CV4 7AL, UK
[r]Dipartimento di Fisica, Università di Roma "Tor Vergata", I-00133 Roma, Italy
[s]Centro de Astrobiología (CAB), CSIC-INTA, 28692, Villanueva de la Cañada, Spain
[t]University of Toronto, Canada
[u]Yale University, New Haven, Connecticut, USA
[v]Cornell University, 122 Sciences Drive, Ithaca - NY, 14850, USA
[w]University of Edinburgh, UK
[x]Dept. of Astronomy, Stockholm University, Sweden
[y]DTU Space, Technical University of Denmark, DK-2800 Kgs. Lyngby, Denmark
[z]Institute for Planetary Research, German Aerospace Centre, 12489 Berlin, Germany
[aa]Space Research Institute of the ÖAW, Graz
[ab]LESIA, Observatoire de Paris, 5 place Jules Janssen, 92195 Meudon, France
[ac]University of Southern Queensland - Montana State University, USA
[ad]Department of Astronomy, Carl Sagan Institute, Cornell University, USA
[ae]Institute of Astronomy, University of Cambridge, Cambridge, CB3 0HA, UK
[af]McGill University, Trottier Space Institute, 3550 Rue University, Montréal, Canada
[ag]Centre Spatial de Liège, Université de Liège, Avenue Pré-Aily, 4031 Angleur, Belgium
[ah]Space research & Planetary Sciences, Universität Bern, 3012 Bern, Switzerland
[ai]Aryabhatta Research Institute of Observational Sciences: ARIES, Nainital, India
[aj]German Aerospace Center (DLR), MUSC, Linder Höhe, 51147 Köln, Germany
[ak]SRON, Netherlands Institute for Space Research, Niels Bohrweg 4, Leiden, The Netherlands
[al]Universidad Nacional de Colombia, Colombia
[am]Network for Life Detection; 2901 Bink Place, Las Cruces, NM, USA
[an]Dep. of Astronomy and Steward Observatory, University of Arizona, Tucson, AZ 85721, USA
[ao]Large Binocular Telescope Observatory, University of Arizona, Tucson, AZ 85721, USA
[ap]Universitäts-Sternwarte, Ludwig-Maximilians-Universität, 81679 München, Germany
[aq]Ateleris GmbH, Switzerland
[ar]Dep. of Astronomy & Astrophysics, University of California, Santa Cruz, CA 95064, USA
[as]Leiden Observatory, P.O. Box 9513, NL-2300 RA Leiden, The Netherlands
[at]Department of Space, Earth and Environment, Chalmers University of Technology, Sweden
[au]Université Paris-Saclay, Université Paris Cité, CEA, CNRS, AIM, Gif-sur-Yvette, France
[av]Bayerisches Geoinstitut, Universitätsstrasse 30, Bayreuth, Germany
[aw]Institut de Radioastronomie Millimetrique (IRAM), 38406 St Martin d'Heres, France
[ax]Instituto de Astrofísica de La Plata, CCT La Plata-CONICET-UNLP, La Plata, Argentina
[ay]Geneva Observatory, Department of Astronomy, University of Geneva, Geneva, Switzerland
[az]Blue Marble Space Institute of Science, Seattle, Washington 98104, USA
[ba]Laboratoire d'astrophysique de Marseille, France
[bb]Department of Astrophysics, University of Zurich, CH-8057 Zurich, Switzerland

[bc]Christian-Albrechts-Universität zu Kiel, Leibnizstr. 11, Kiel, Germany
[bd]CITEVA, Universidad de Antofagasta, Chile
[be]University of Exeter, Astrophysics Group, Stocker Road, Exeter, EX4 4QL, UK
[bf]Institute of Space and Astronautical Science, 3-1-1 Yoshinodai, Sagamihara, Japan
[bg]Nagoya University, Furo-cho, Chikusa-ku, Nagoya 4648602, Japan
[bh]INAF - Astronomical Observatory of Trieste, Italy
[bi]Center for Star and Planet Formation, Globe Institute, University of Copenhagen, Denmark
[bj]Department of Physics, Astronomy and Mathematics, University of Hertfordshire, UK
[bk]Dep. of Earth and Planetary Sciences, University of California, Riverside, CA 92521, USA
[bl]University of Belgrade-Faculty of mathematics, Dep. of astronomy, 11158, Belgrade, Serbia
[bm]Technical University of Munich, Dep. of Aerospace and Geodesy, 80333 Munich, Germany
[bn]Cosmic Origins Of Life (COOL) Research DAO, coolresearch.io
[bo]Faculty of Physics, University of Duisburg-Essen, Germany
[bp]Physikalisches Institut der Universität zu Köln, 50937 Köln, Germany
[bq]INAF - Osservatorio Astrofisico di Catania, via S. Sofia, 78 - 95123 Catania, Italy
[br]Tartu Observatory, University of Tartu, Toravere, 61602 Tartumaa, Estonia
[bs]University of California, Riverside, 900 University Ave., Riverside, USA
[bt]TUDelft, Faculty of Aerospace engineering, Kluyverweg 1, 2629 HS Delft, NL
[bu]Department of Astronomy Astrophysics, University of Chicago, Chicago, USA
[bv]Eberly College of Science, Penn State University, University Park, PA, 16802, USA
[bw]National Institute of Science Education and Research, Jatni 752050, Odisha, India
[bx]Homi Bhabha National Institute, Training School Complex, Mumbai 400094, India
[by]Univ. Grenoble Alpes / CNRSQ / IPAG, France
[bz]Campo Catino Observatory, Regione Lazio, Italy
[ca]University of Washington, 3910 15th Ave NE, Seattle, WA, 98195-1580, USA
[cb]Jet Propulsion Laboratory, California Institute of Technology, Pasadena CA 91109 USA
[cc]University of Michigan, Ann Arbor, MI USA
[cd]NOVA optical infrared group at ASTRON, Dwingeloo, NL
[ce]Max Planck Institute for Astrophysics (MPA), Garching, Germany
[cf]Department of Physics, Faculty of Science, Kyambogo University, Kampala, Uganda
[cg]Instituto de Astrofísica e Ciências do Espaço, Universidade do Porto, Porto, Portugal
[ch]School of Aeronautics and Astronautics, Purdue University, Indiana, USA
[ci]Instituto de Astrofisica de Canarias, Spain
[cj]CTO of Heliospace Corporation, 2448 Sixth St, Berkeley, CA, USA
[ck]The Mathematical Institute of the Slovak Academy of Science,Bratislava, Slovakia
[cl]Landessternwarte, ZAH Universität Heidelberg, 69117 Heidelberg, Germany
[cm]University of Central Florida, Physical Sciences Building 106, Orlando, Florida, USA
[cn]Institut für Astrophysik und Geophysik, Georg-August-Universität, Göttingen, Germany
[co]Institute of Space Sciences (ICE, CSIC), C/Can Magrans, s/n, 08193 Bellaterra, Spain
[cp]Institut d'Estudis Espacials de Catalunya (IEEC), 08660 Castelldefels, Spain
[cq]Department of Astronomy, Yale University, New Haven, CT 06520, USA
[cr]Disruptive Space Technology Centre, RAL Space, STFC-RAL, Didcot, UK
[cs]SRON Netherlands Institute for Space Research, Groningen, NL
[ct]Nicolaus Copernicus Astronomical Center, Polish Academy of Sciences, Warsaw, Poland
[cu]Vanderbilt University, Department of Physics & Astronomy, Nashville, TN 37235, USA

[cv]AIU, Friedrich Schiller University, 07745 Jena, Germany
[cw]Delhi Technological University, Delhi, India
[cx]Space Astronomy Group, U R Rao Satellite Centre, Bengaluru, India
[cy]University of Lethbridge, 4401 University Drive W, Lethbridge, Alberta, Canada
[cz]Johns Hopkins University, 3400 North Charles Street, Baltimore, MD 21218, USA
[da]The University of Tokyo, Graduate School of Science, Hongo 7-3-1, Bunkyo-ku, Tokyo, Japan
[db]Harvard University, 26 Oxford St., Cambridge, MA, USA

ABSTRACT

The Large Interferometer For Exoplanets (LIFE) is a proposed space mission that enables the spectral characterization of the thermal emission of exoplanets in the solar neighborhood. The mission is designed to search for global atmospheric biosignatures on dozens of temperate terrestrial exoplanets and it will naturally investigate the diversity of other worlds. Here, we review the status of the mission concept, discuss the key mission parameters, and outline the trade-offs related to the mission's architecture. In preparation for an upcoming concept study, we define a mission baseline based on a free-formation flying constellation of a double Bracewell nulling interferometer that consists of 4 collectors and a central beam-combiner spacecraft. The interferometric baselines are between 10–600 m, and the estimated diameters of the collectors are at least 2 m (but will depend on the total achievable instrument throughput). The spectral required wavelength range is 6–16 µm (with a goal of 4–18.5 µm), hence cryogenic temperatures are needed both for the collectors and the beam combiners. One of the key challenges is the required deep, stable, and broad-band nulling performance while maintaining a high system throughput for the planet signal. Among many ongoing or needed technology development activities, the demonstration of the measurement principle under cryogenic conditions is fundamentally important for LIFE.

Keywords: Nulling, Interferometry, Space, Mission, LIFE, exoplanets

1. INTRODUCTION

Some of the key goals of modern astrophysics include understanding the nature and diversity of terrestrial-type exoplanets, determining whether and how such objects could be habitable, and addressing the question "Are we alone?". To achieve these goals, we require ways to probe the spectra of a large number of temperate terrestrial exoplanets. Currently, we have obtained information about small exoplanets only for a limited number of transiting objects through transmission spectroscopy or secondary eclipse observations with telescopes such as the James Webb Space Telescope (JWST).[1–4] Yet these are worlds far different from our own as they typically orbit around low-luminosity M-stars and feature much warmer conditions. Even for the most promising objects a detailed atmospheric characterization and the search for biosignatures is extremely challenging[5] and investigating systems similar to Sun-Earth is not achievable using existing methods and current instruments.

As seen from Earth, most exoplanets do not transit their host stars. Consequently, the search and characterisation of these systems require direct imaging techniques that can access the spectra of a planet directly. To enable this observing technique three criteria need to be met: high contrast to remove most of the light of the host star, high angular resolution to separate the planet signal from that of the star, and high sensitivity in order to collect the relatively few photons from the planet. While there are a few instruments being developed for ground-based telescopes that should detect a handful of planets (such as METIS on the Extremely Large Telescope[6]), the last requirement indicates that this objective is best suited for a space mission. Based on the 2020 decadal survey from the US astronomy community, a large, UV to NIR coronagraphic space telescope, currently called the Habitable Worlds Observatory (HWO), is being pursued by NASA, aiming to achieve the necessary contrasts of 10^{-10} to image an Earth-like planet around a Sun-like star in reflected light at optical wavelengths.[7]

However, there is another path forward that leverages the relatively lower contrast requirement in the mid-infrared (MIR) spectral band: a space-based nulling interferometer. Nulling interferometry is a concept whereby

Further author information: (Send correspondence to glauser@phys.ethz.ch)

two or more separate apertures are combined with relative phase shifts imposed between the different beam trains, such that light from the on-axis target (i.e., the system host star) is destructively interfered while light from the off-axis target (i.e., the exoplanet) is constructively interfered. The angular separation of the first constructive maximum depends on the wavelength and the separation distance of the apertures (the nulling baseline). This baseline can be optimized for each target, e.g., to maximize the detection yield of planets within the habitable zone. One prominent concept of nulling interferometer is the double-Bracewell interferometer[8] where the light of four apertures is first nulled pairwise by introducing an achromatic π-phase shift before it is cross-combined with the other pair with an additional $\pi/2$ phase offset. Because the apertures are spatially sufficiently separated, nulling interferometry can provide the angular resolution required while working at MIR wavelengths. The idea of a space-based MIR nulling interferometer is not new, having been pursued by both NASA and ESA in their TPF-I[9,10] and *Darwin*[11,12] mission concepts in the early 2000s. Unfortunately, due to a lack of clarity on the scientific yields of the missions and low technological immaturity, both missions were abandoned by the end of the 2010s.

Since 2017, there has been a revival of the idea in the form of the Large Interferometer For Exoplanets (LIFE), a space mission leveraging the heritage from TPF-I and *Darwin*, but folding in new technologies and the current knowledge of exoplanet science. The project has been gaining significant momentum worldwide as showcased by a rapidly growing number of papers published in the LIFE paper series.[13–24] Furthermore, thanks to LIFE, the topic of directly detecting small temperate exoplanets at MIR wavelengths is featured as a candidate for a future mission in the Voyage 2050 program of the European Space Agency ESA.[25,26]

In this paper, we aim to provide the community with a summary of the current baseline concept of LIFE, covering the key requirements and preliminary architecture of the collectors and combiners. We also describe the ongoing technological development for the mission, and current open questions and tradeoffs that are required for the adoption of mission parameters.

2. KEY MISSION PERFORMANCE REQUIREMENTS

Most requirements for the LIFE mission presented in the following are either derived through simulations carried out within the LIFE team or, where still valid, they are inherited from the former *Darwin*/TPF-I concepts. In the final stages of the *Darwin* and TPF-I concept phases, both missions converged on very similar mission baselines (see Section 3.1). The requirements of both concepts were derived based on science goals which required the detection and characterization of a specific number of Earth-like exoplanets in the habitable zone (HZ). For *Darwin* it was $\sim$ 25 Earth-like exoplanets,[12] for TPF-I it was searching 150 HZs with 90% completeness.[27] Furthermore, the capability to detect habitability tracers and bio-signatures in the atmospheres of these planets was required. As empirical occurrence rates of rocky habitable zone planets were not available at that time, the teams relied mainly on comparative studies which preferred concepts that provided higher completeness (the ability to detect an exoplanet if it is present) in the habitable zones of their target stars. While useful in itself, this approach could not quantitatively link the number of detected and characterized exoplanets to key mission parameters.

In the decade following the conclusion of *Darwin* and TPF-I, two advances in the field revived the space-based mid-interferometry community and subsequently allowed us to formulate the missing link in the mission requirement discussion. Firstly, while the Kepler mission did not fully meet its objective to statistically measure the frequency $\eta_\oplus$ (occurrence rate) of Earth-sized planets in the HZ around Sun-like stars,[28] subsequent analyses were able to provide robust estimates on $\eta_\oplus$.[29–33] Using these estimates, work carried out by the LIFE team commenced to connect key mission parameters to the expected rocky exoplanet yield in the habitable zone[13,18,34] (see Figure 1 left) using the custom-built mission simulation tool LIFEsim.[14] Secondly, advances in the atmospheric modeling of terrestrial planets as well as multi-parameter fitting techniques enabled so-called spectral retrievals of Earth-like planets in the mid-infrared. Synthetic spectra of solar system terrestrial planets are used to constrain the quality of the spectra (in terms of noisiness, wavelength coverage, and spectral resolution) needed to robustly retrieve relevant planetary properties (radius, ground pressure, and temperature) and atmospheric constituents (e.g., CO_2, O_3, CH_4, H_2O).[15,35] This approach was subsequently empirically validated on disk-integrated Earth spectra observed from Earth observation satellites.[36] Table 1 provides a snapshot of the current key mission requirements and performance metrics, the components of which will be elaborated on

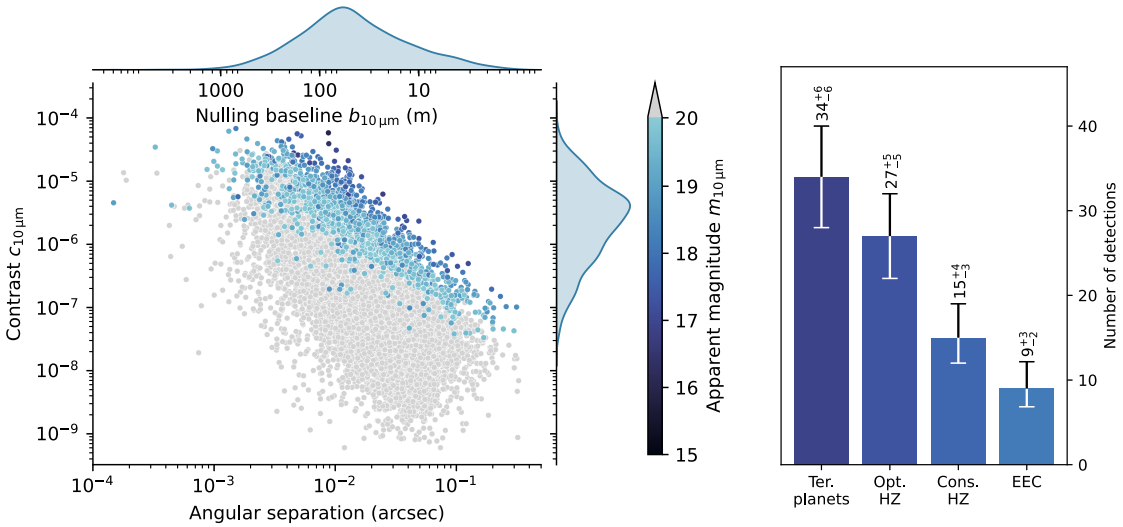

Figure 1. *Left:* Illustration of how the results of the Kepler mission inform key mission parameters of LIFE. Points plotted are an artificial rocky planet population based on Kepler statistics[32,37] occurring in their respective habitable zones generated using P-Pop.[34] We plot their respective star-to-planet flux contrast ratio measured at 10 μm over the angular separation at which they occurred. The colors trace the planet's apparent 10 μm Vega-magnitude and planets with $m_{10\mu m} > 20$ are plotted in gray. The nulling baseline length required to achieve a certain angular resolution is shown. *Right:* Yield predictions with the setup specified in Table 1. The yields are based on artificial planet populations described in Kammerer et al. (2022).[18] Shown are the expected number of detections around F-, G- and K-type stars within the distance up to 20 pc for all terrestrial exoplanets ($0.5R_\oplus < R_p < 1.5R_\oplus$), terrestrial exoplanets in the optimistic and conservative habitable zone[38] and for exo-Earth candidates (EEC, $\sim 0.8R_\oplus < R_p < 1.4R_\oplus$ in conservative HZ).

further in Section 3. Figure 1 illustrates how adopting these parameters yields exoplanet detection numbers as specified in the science objective.

3. MISSION BASELINE CONCEPT

We now report on the LIFE mission baseline concept. Several building blocks of LIFE are reincarnations of ideas from the various *Darwin* and TPF-I studies, modified for the present understanding of the available technologies and needs for LIFE. This section is divided into three components, where we will discuss the architecture of the mission in general; the concept of the collector spacecraft; and the concept of the combiner spacecraft including one implementation of the internal optical train.

3.1 Configuration

3.1.1 The Emma X-array

The overall baseline configuration of LIFE is that of a double Bracewell interferometric nuller in an "Emma X-array" configuration. The double Bracewell was an extension of the original nulling interferometer[8] by Angel and Woolf (1997).[39] This concept consists of four telescopes, with a nulled output being produced by two pairwise combinations of the telescopes. These two nulled outputs are then further mixed to produce deeper and broader nulls. To detect the planet, the array is rotated so that any off-axis sources are modulated, but the on-axis star and incoherent background sources remain static.

In the *Darwin* and TPF-I studies,[40] it was realized that having the four telescopes in a rectangular formation allows for high angular resolution along the long "imaging" baseline, and then shorter "nulling" baselines that prevent the star from being too resolved in the null. This geometry can be seen in Figure 2. The configuration also allows an equal amount of propellant to be used during the rotation, and a simpler geometry for combining the beams. This formation is finally augmented by the "phase-chopping" modulation, where the two nulled outputs are mixed with a $\pm\pi/2$ phase shift and swapped on the timescale of 0.01 to 1 Hz.[41] This chopping

Table 1. Key mission parameters and requirements for LIFE.

Item	Value	Rationale or comment
Array		
# collector spacecraft	4	Minimum number with which robustness against instrumental noise is achievable with baseline beam combiner
Nulling baseline	10 - 100 m	Lower limit for nulling of nearest S6un-like stars, upper limit for nulling of M-type star at 10 pc. Lower limit also influences minimum spacecraft separation.
Imaging baseline	60 - 600 m	Moves planet modulation to higher frequencies to mitigate impact of low-frequency instability noise. Upper limit also influences maximum spacecraft separation.
Combiner spacecraft	Out of plane	Field of regard covers full sky, lower complexity in collector spacecraft
Modulation	Rotation & Phase chopping	Rotation for localization of planets and fuel efficiency, phase chopping for detector and incoherent light calibration
Temperature	$\leq$ 45 K	Suppression of the thermal radiation from the collector mirror
Instrument		
Beam combiner	Double Bracewell	Realizable with high technology readiness level (TRL) bulk optics, noise properties for instability noise
Wavelength coverage	6.0 - 16 µm (goal 4.5 – 18 µm)	To include H_2O absorption feature above 17 µm and resolve H_2O and CH_4 features at 7.7 µm in Earth-like atmosphere[15]
Resolving power	>100	CH_4 detection in Earth-like atmosphere (Konrad et al. 2024)
Sensitivity*	$S_{10\mu m} = 0.4\,\mu$Jy in 4 days	Required to detect and characterize 30 rocky planets in the habitable zone of sun-like stars within the mission lifetime
Contrast*	Null depth 10^{-5} Null stability rms 10^{-8}	
Temperature	$\leq$ 15 K	Suppression of the thermal radiation from the collector internal structure and optics
Mission		
Lifetime	$\geq$5 years	Required to detect and characterize 30 rocky planets in the habitable zone of sun-like stars within the mission lifetime

* evaluated at $10\,\mu$m and $R = 100$

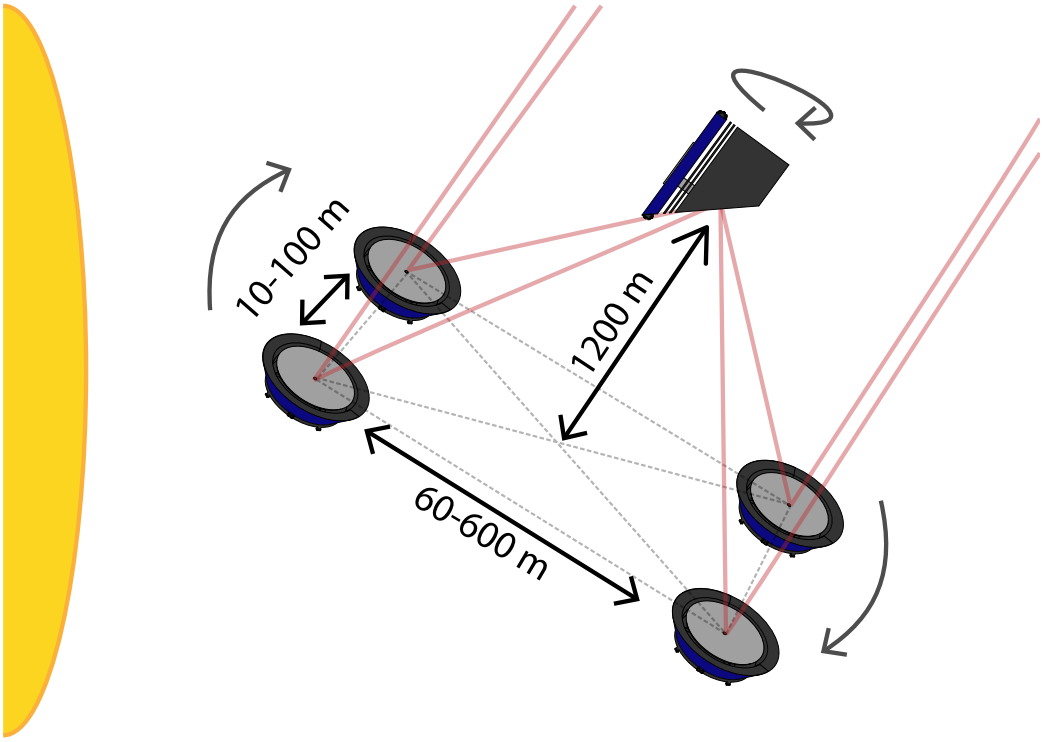

Figure 2. Baseline LIFE configuration: the Emma X-array. The collector telescopes are arranged in a 6:1 rectangle and rotated along the star pointing axis. The combiner is out-of-plane of the collectors and co-rotates with the array, resetting the rotation every 90° to ensure the radiation shield is always facing the Sun.

allows any irregularities in the detector and uneven zodiacal background leakage to be calibrated out, and taking the difference of the two outputs (a so-called "differential null") minimizes the sensitivity to any symmetrical background noise (e.g zodiacal light, symmetrical exozodiacal disks, symmetrical stellar leakage).[41,42] Lay (2006),[43] also showed that having a 6:1 imaging to nulling baseline ratio allows for reduced sensitivity to instability noise; that is, dynamic fluctuations in the null-depth due primarily to stellar leakage. For LIFE, we have nominally adopted imaging baselines spanning from 60 to 600 m, stemming from an assumption of a 10 m minimum separation between spacecraft (to avoid collisions) and a 600 m maximum separation (to ensure we can still keep metrology links).[13]

The "Emma" component of the Emma X-array concept corresponds to the 3D nature of the configuration. Each of the collectors is flown in the same plane, lying on the surface of a large parabola perpendicular to the star-pointing vector. The combiner spacecraft is located out of this plane, towards the star; this allows the collectors to be simple mirrors rather than a telescopic system, equivalent to an M1 mirror for a monolithic telescope. As the collectors rotate, the angle of incidence will vary slightly inducing a set of dynamic aberrations including astigmatism and polarisation that must be compensated inside the combiner. Following past work,[44] we have nominally placed the combiner to be located 1,200 m above the plane of the collectors to reduce the magnitude of these effects. This can also be seen in Figure 2.

3.1.2 Field of regard and modulation

The LIFE mission is assumed to be located at the second Lagrange point of the Sun-Earth system (L2), due to its orbital stability for formation flying and the thermal stability required for cryogenic missions. Now, due to the three-dimensional arrangement of the array, the immediate field of regard is limited by the need for passive cooling and correspondingly, the need for shielding the cold optics from the sun. Further, the target direction and the optical beams between the spacecraft need sufficient angular separation from the sun-pointing vector. Also following from previous *Darwin* and TPF-I studies, we adopt that the array can point in an annulus between

∼45° and ∼85° from the anti-sun angle.[12,44] This allows ∼99% of the sky to be covered over a year as the Earth revolves around the Sun (the ecliptic poles being inaccessible), with a minimum continuous observing time for a given target of 38 days. Now, work is still ongoing as to whether the full sky does need to be covered, with investigations into so-called "golden targets" and synergies with the Habitable Worlds Observatory target list.[22,45] Further restricting the field of regard may allow a loosening of technical requirements, specifically with regard to thermal, optical and propulsion considerations. However, unless a definitive scientific rationale appears such that LIFE does not need full sky coverage, we assume that maximizing the field of regard is necessary.

For modulating the planet signal we define it as a baseline operation scheme that the array rotates around the star/pointing axis. The collectors and combiner are also assumed to co-rotate with the array so that any differential polarisation and aberration effects are minimized. To maintain that the radiation shield of the combiner is facing the sun, the combiner will likely need to reset the rotation every 90°.

However, there exists an open question as to whether the described modulation scheme is indeed the most efficient modulation method in terms of both, observing efficiency and propulsion. Indeed, certain post-processing methods[23] may allow for the planet to be retrieved with a reduced amount of modulation. Further study into the coupling between specific propulsion methods and the efficiency of planet signal modulation is likely warranted.

3.1.3 Alternate configurations

We briefly address the notion of other telescope configurations with varying numbers of telescopes, in particular, that of five telescopes in a pentagonal formation. This concept was looked at by Hansen et al.[16,19] and found to hold comparable science yield to that of the double Bracewell, especially in that it is more capable of removing stellar leakage. However, the immaturity of the beam combiner concept necessary for a five telescope nuller,[19,46] certainly in comparison to the Modified Mach-Zehnder concept (MMZ; see Section 3.3), means that at this stage the baseline configuration is set at four telescopes.

Finally, there is also a question as to whether the combiner should be in-plane with the collectors. This would require the collectors to be telescopes rather than single mirrors, which is a trade-off discussed in the next section. Nevertheless, an in-plane concept results in a far more limited sky-coverage, as the array must point around the anti-sun vector, and the combiner also will see more of the warm components of the collectors. Together, we thus assume an out-of-plane concept for the combiner.

3.2 Collectors

The baseline LIFE collector concepts are adopted from the TPF-I Emma concept.[44,47] They consist of a single spherical mirror that is cooled to below ∼45 K, to minimize the thermal background radiation from the collector mirror. An annulus surrounding the collector mirror will also need to be cooled to minimize thermal stray light from the surrounding structure that leaks through the cold stop in the combiner due to diffraction. The mirror is surrounded by a radiation shield, which due to the co-rotation of the collectors with the array is required to fully surround the primary mirror. This is a deviation from the TPF-I Emma concept which had an asymmetric concept to radiate heat out the far side of the spacecraft to assist with passive cooling; alternative radiator concepts are being considered for LIFE. The scattered thermal light from the collectors is a major source of noise for the mission, and as such it is critical that a structural, thermal, and scattered light model is established soon to quantify this noise contribution.

The side facing the sun is also fitted with solar panels for power. A sketch of the collectors can be seen in Figure 2. Our baseline assumption for the diameter of the collector mirrors is 2 m, although this is likely to change depending on more detailed demonstrations of realistic instrumental throughput and the desired sensitivity of the mission.

One of the key investigations required for the collectors is that of formation flying stability, as while optical path differences (OPD) can be compensated for inside the combiner, there will be limited stroke and the OPD positional information should ideally be within the coherence length of the instrument to avoid long fringe scans. Under an assumption of a spectral resolution on the order of 100, this leads to a coherence length of about 1 mm at 10 µm. We hence assume that we require positional knowledge along the optical path within 1 mm, with the other axes being acceptable at the 1 cm precision level. This can be achieved with formation flight stability at

the cm level, with higher precision metrology along the optical path axis. Section 4.1 discusses the ongoing and planned activities with regard to the technological developments for formation flying.

Now, having a single spherical mirror as a collector raises some optical complications that need to be addressed, specifically intrinsic aberrations that will propagate through to the combiner. The variable optical path from being out-of-plane will also induce polarisation differentials and pupil rotation; it is this latter point we aim to minimize through having the combiner co-rotate with the array. The aberrations and polarisation differentials will aim to be compensated through deformable mirrors (DMs) and a polarisation compensator on the combiner and will be discussed in the next section. Nevertheless, it is possible that even with these compensators, there will be both residual static aberration and non-linear polarisation mismatch that will inherently limit the achievable contrast. Investigations into the magnitude of these residual errors should be a priority to ensure a single mirror collector is a viable option.

This leads to the question of a telescopic system, and whether the collectors should be afocal telescopes and transmit a corrected, collimated beam to the combiner. While this concept has not been discarded and has benefits in terms of the quality of the transmitted beam, there are several complications that render such a system less desirable than a single mirror. Firstly, a telescopic system increases the complexity of each of the collectors; the telescope would likely require numerous more reflections and more thermal management to avoid contaminating the beam with emitted thermal radiation. A wavefront sensor and DM would still be necessary for aberration correction, essentially moving the components from the combiner to the collectors, and so in total, it greatly increases the launch size and mass of the four collectors. With increased masses comes naturally the need for an increase of the propellant fuel required for the array rotation. Finally, Fresnel diffraction with a collimated beam results in a loss of fiber coupling at long wavelengths, and so a very large beam size would need to be maintained to minimize this effect. In total, the benefits of a telescopic collector at this time do not outweigh the problems they induce, and unless the aforementioned residual optical aberrations become limiting, it is assumed LIFE will consist of single mirror collectors.

3.3 Combiner

We now turn to the baseline concept for the beam combiner. The spacecraft concept is again mainly taken from the TPF-Emma studies,[44,47] with one large sunshade and radiation shields facing the Sun and four large apertures for the collectors to inject into the combiner. This can be seen in Figure 2. The whole beam combination unit will by cryogenically cooled to approximately 15 K to minimize the impact of the instrument thermal background. As mentioned in Section 3.1, the combiner is envisioned to co-rotate with the collectors to minimize differential polarisation effects, with the rotation resetting every 90° for the sunshade to remain pointing at the Sun.

The rest of this section is dedicated to walking through and discussing the various components of the baseline optical concept of the combiner, which is shown in Figure 3. It should be noted in advance that this combiner system combines the naive inclusion of several rather complex subsystems to provide here an overview of the possible building blocks of the LIFE combiner; future trade-offs and subsystem-level demonstrations will likely prove multiple components of this "all-inclusive" concept redundant, and various subsystems could likely be implemented more efficiently. Nevertheless, this concept is useful as a starting point for discussing the requirements on the combiner and identifying components for further development. This concept is a convergence between multiple other existing concepts, such as that of TPF-I[47] and of the various *Darwin* industry studies.

3.3.1 Receiving optics

To begin with, the collectors propagate the non-collimated light to the combiner spacecraft, where it is then directed into the beam train by a set of four steering mirrors (one per beam). These mirrors may also be able to be moved laterally to implement an optical path difference between arms, thus functioning as a preliminary coarse delay line. The beam then passes through some form of polarisation compensator to remove the geometrically induced polarisation difference between the beams. One of the simplest ideas is to have two fold mirrors, angled such that the intermediate beam is anti-parallel to the star vector. This thus cancels out the geometric polarisation distance. As the combiner rotates, this set of optics should also rotate such that the polarisation remains corrected at all azimuth angles.

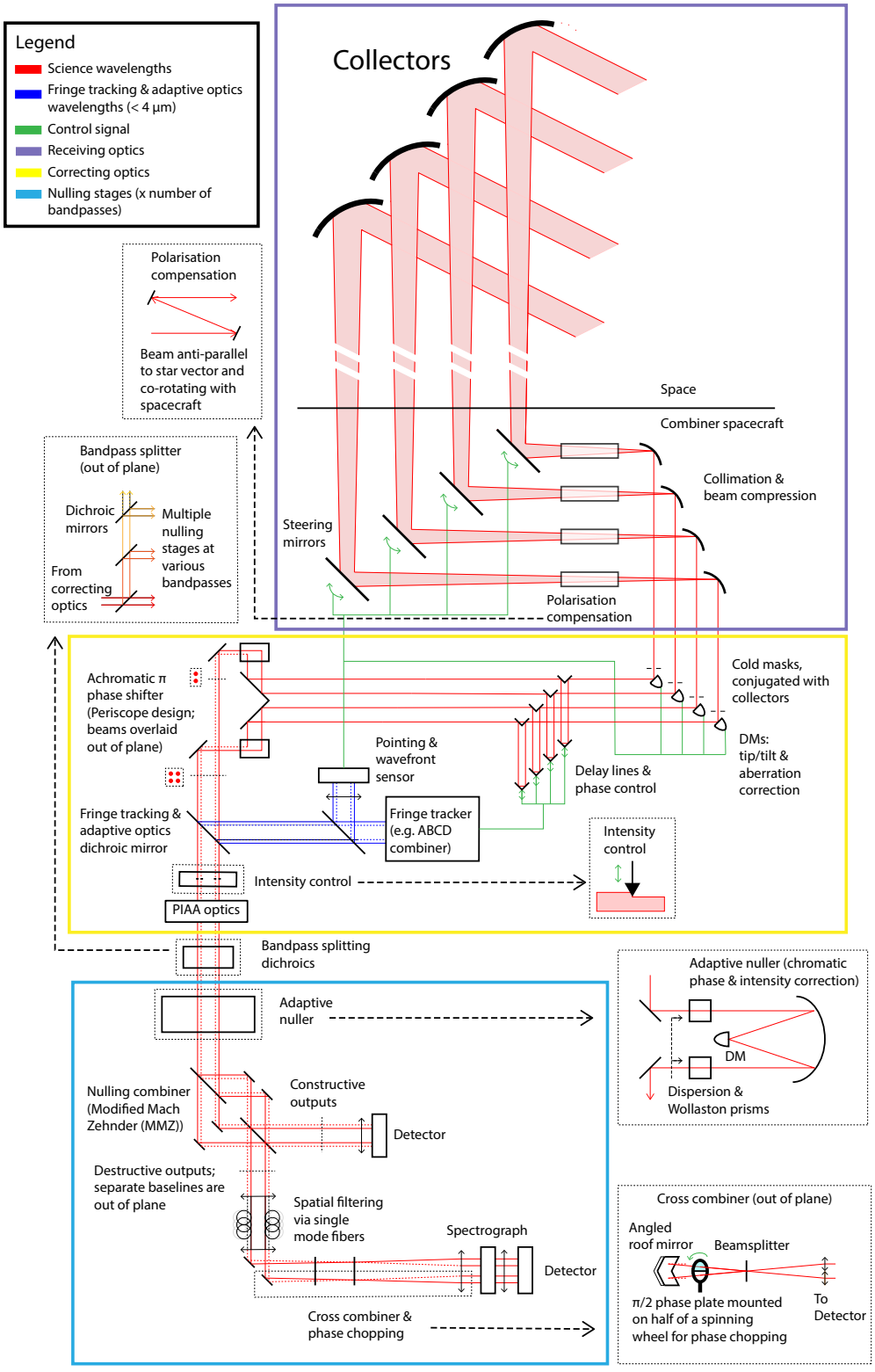

Figure 3. The baseline LIFE combiner architecture. This is described in detail in Section 3.3.

3.3.2 First stage of correcting optics

The beams then come to an off-axis parabola which collimates and compresses the beam into a more usable size. The beam then falls onto a set of DMs with a nearly co-incident cold pupil stop, conjugated with the collector mirror. The DM corrects for the spherical and astigmatism aberrations induced by the spherical collectors. These DMs also have several other purposes, including correcting for tip/tilt, and also potentially acting as a fast delay line in conjunction with the steering mirrors. One major investigation that remains is looking into the stroke, response time, and space and cryogenic compatibility of these DMs, and whether they can serve as the multi-functional devices that are currently envisioned.

From here, the corrected beams may now be fed into delay lines, which co-phase the beams. However, whether a dedicated delay line system is strictly needed considering the potential delay line capabilities of the previous two dynamic mirrors remains to be seen. This will need to be a trade-off between the required performance of the cryogenic DM and a greater number of optical elements. Furthermore, the delay line as sketched in Figure 3 could be designed more efficiently with fewer reflections; the depicted "trombone" design is mainly for functional clarity.

3.3.3 Achromatic phase shifter

To destructively interfere the on-axis beams, we require an achromatic π phase shift to be induced between the telescopes in each of the nulling baselines. One such method is through the use of a three-mirror periscope,[48] which relies on the polarisation inversion during an optical reflection: If the reflections of two beams in a 3-mirror periscope are mirrored with respect to each other, the resulting polarisation is relatively rotated by 180°, which corresponds to an effective π-shift that is intrinsically achromatic. Other methods for building achromiatic phase shifters were proposed[48] and experimentally compared,[49] while the three-mirror periscope appeared to be the most robust method. Nonetheless, this implementation does impose strict polarisation and alignment control, which thus is foreseen to be demonstrated in a cryogenic environment.[50]

3.3.4 Control stage

The beam train then goes through a dichroic mirror, where light is split between the science wavelengths (>4 µm) and control wavelengths (<4 µm). The shorter wavelengths are then further split and used by two subsystems. The first is a fine pointing and wavefront sensor; this is used to control the DMs and steering mirrors to obtain a well-aligned, undistorted beam. The second component is the fringe tracker, whose job is to maintain the OPD between the beams at zero. This requires another interferometric beam combiner to measure the phase of the fringes and then control either the dedicated delay lines or else also contributing to the control of the optical path axis of the steering mirrors and DMs. One such implementation of the fringe tracker is a photonic ABCD device working in the K band ($\sim$ 2 µm) such as that used by the GRAVITY instrument at the Very Large Telescope Interferometer (VLTI).[51]

A metrology system tracking movements internal to the nulling stage will also be valuable to ensure high fiber coupling and stable injection. To have the beam propagate through, and for it not to be mixed with the science wavelengths, the control dichroic should allow a small amount of short wavelength light through. An example of such a metrology system can be found in Paper 13095-115 (Birbacher et al., 2024). We note that this is not included in Figure 3 for clarity purposes.

3.3.5 Second stage of correcting optics

The science wavelengths continue onwards to an intensity control subsystem, where small actuators can insert themselves into the light path to reduce the relative intensity between the beams. This subsystem is controlled via the nulling detector, where maximum contrast is achieved with equal-intensity beams. However, this particular control system may also be not strictly necessary if an adaptive nuller (described later) is able to be implemented.

For high levels of coupling into the spatial filters at the end of the nuller, the beam will likely need to be apodized. As such, we foresee that a set of phase-induced amplitude apodization (PIAA) optics may be required. This is a technique whereby the beam is apodized by a pair of precisely shaped aspheric optics, thus shaping the beam such that it maximizes fiber coupling without loss of transmission.[52] The field of view of PIAA optics is very small, however, and so these optics should be placed after the pointing sensor.

This is the last common subsystem before the science light is split into the various sub-bandpasses, the size and location of which will depend on the available technology of the following components. This light could be split through a series of dichroics that are out of the plane of the diagram in Figure 3, essentially producing a number of copies of the nulling stage (highlighted in blue) for different wavelengths and stacking them on top of each other.

3.3.6 Adaptive nuller

Inside each of the nulling bandpasses, we begin with one of the more complex subsystems: the adaptive nuller. First demonstrated by Peters et al. (2010),[53] this system is designed to provide a wavelength and polarisation-dependent phase and amplitude modulation, thus correcting any static deficiencies of the nuller. The light is dispersed spectrally and into two linear polarisations via a dispersion and Wollaston prism, before being reflected onto a DM. The DM can modify the phase of the beam at each wavelength channel via the piston, as well as an intensity adjustment through tip/tilt. This latter functionality works due to the spatial filter at the end of the nuller; by adjusting the tip/tilt of the beam, the pupils are misaligned and the intensity decreases. The light from the DM is then sent backward through the prisms such that the light is one collimated beam again. Due to the likely lossy nature of the dispersive elements, and the fidelity required from the DM, another demonstration of the adaptive nuller would be very valuable in ensuring the high system transmission and that the technology readiness level (TRL) is achieved.

3.3.7 Nulling and spatial filtering

The nulled outputs will be produced through a modified Mach-Zehnder combiner, where each beam is combined through a symmetric number of reflections and transmissions.[48] Hence the nulled outputs are robust against uneven splitting ratios. The two nulling baselines are combined in the same MMZ but offset out of the plane of the diagram. The constructive outputs can be imaged on a detector for usage in intensity monitoring, and the destructive outputs are then propagated further.

After nulling, the beams need to be spatial filtered so that only the fundamental spatial mode is measured, minimizing the impact of any wavefront aberrations on the null. This is also critical, as otherwise small local variation in the wavefront will prevent deep contrasts from being achieved. We put the spatial filters here, between the nulling combiner and cross combiner, to avoid having any aberrations in the cross combiner mimicking a planet signal. To spatial filter the beams, the light is coupled into a single-mode fiber or similar photonic waveguide through the use of an off-axis parabola. We note here that this is one of the major technical challenges ahead; MIR photonics is not a very mature field, and high-throughput spatial filters at wavelengths longer than 10 µm have not been adequately demonstrated to the necessary TRL.

3.3.8 Cross combination and spectrograph

The final combination step is mixing the two nulled baselines. This can be done by folding the beams, collimated from the output of the spatial filter, off a roof mirror before entering a final beamsplitter. To induce the differential null and provide phase chopping, one of the beams needs to undergo a $\pi/2$ phase shift. One way of implementing this is to produce an achromatic $\pi/2$ phase plate[54,55] and insert it into half of a spinning chopper wheel. Chopping can then be induced by spinning the wheel and changing which of the two input beams undergoes the phase shift. Notably, as the nulling is done in the previous MMZ, the beam splitter and phase shift do not have as strict requirements for obtaining high contrast. Questions remain as to whether such a phase plate can be produced that works with minimal residuals at a non-zero angle of incidence. An alternative phase chopping method would be to implement a beam switcher that swaps which of the two nulled outputs undergoes the phase shift, although a stable, cryogenic implementation of this may be more difficult than the proposed phase plate method.

After cross-combination, the nulled beam is spectrally dispersed to a spectral resolution of around 100. Depending on the wavelength this is achieved ideally using prisms to prevent higher-order losses when using gratings.

3.4 Detectors

The detectors are the final element in the complex light collection, modulation, and detection chain necessary for LIFE. The detection of the sparse exoplanet signal after nulling the host star takes place in a photon-starved regime. Hence, the performance of the detectors has to be up to par with this task. While several detector characteristics will influence the performance, in particular the response stability, read-out noise and dark current are key performance parameters to consider. For the required dark current, different values were published in the past but recent reevaluation of this parameter let to a rough upper limit in the order of $\sim$1 e^-/s/px.

The standard technology for many years has been Si:As detectors and state-of-the-art devices are being used in the MIRI instrument at JWST. The dark current reported for them reaches down to 0.03 e^-/s/pixel.[56] It remains an open question at this stage however if the required stability for LIFE is comparable to the MIRI detector performance. Unfortunately, there are indications that this detector technology might not be available anymore in the future at the required quality[57] and alternative devices need to be identified.

Originally used mainly for the near-infrared range, Mercury-Cadmium-Telluride (MCT) alloy detectors have found their way into the mid-infrared regime in recent years. The upcoming NEO Surveyor (NASA) and the Ariel (ESA) astrophysics space missions will feature MCT detectors reaching out to 9.6 µm (dark current 0.22 e^-/s/px)[58] and 7.8 µm (dark current 0.07 e^-/s/px),[59] respectively. For ground-based instrumentation, MCT detectors with 13 µm cutoff ("GeoSnap") are being developed.[60] It is possible to tune the MCT stoichiometry to reach longer and longer cutoff wavelengths. Recent experiments with MCT devices with $\lambda_{\mathrm{cutoff}} > 15$ µm demonstrate[61] that quantum effects like quantum tunneling become important. Furthermore, as the Mercury fraction increases with longer cut-off wavelengths the arrays become softer and more prone to defects adversely affecting the dark current. The dark current performance of these first experimental long-$\lambda_{\mathrm{cutoff}}$ devices might exceed the needs of LIFE. One way to improve the performance of such devices is to couple them with optimized readout/amplification electronics, for instance, capacitive trans-impedance amplifier (CTIA) multiplexer read-outs. Using such a circuit for the $\lambda_{\mathrm{cutoff}} = 13$ µm devices, a dark current as low as 0.1 e^-/s/px was achieved.[62] As for wavelengths at the long end of LIFE it remains an open question at this stage if MCT detectors could be also used.

Alternative technologies such as Kinetic Inductance Detectors (KIDs) or superconducting nano-wire single-photon detectors (SNSPDs) are very interesting, although not yet well explored in the MIR.[63–65] While their capabilities for single-photon counting or photon energy resolution might not directly apply to the measurement of LIFE, they could provide a new level of stability and photometric accuracy that would be very well aligned with the needs of LIFE. Their downside might be the required operating temperatures down to the sub-Kelvin regime that requires complex cooling systems. In the past, more conventional ^{3}He sorption coolers were used to reach this level for instance in the Herschel Space Observatory[66] of ESA. In case these refrigerators are open-cycle coolers (like for the Herschel instrument PACS), the lifetime of the mission were strongly affected, and regular recycling of the cooler liquid probably would inhibit long measurement sessions for LIFE. Interestingly, a first in-space demonstration of a more complex approach employing adiabatic demagnetisation (AD) as a refrigerator concept has been previously shown on board of the Japanese Hitomi X-ray mission.[67] This technology has, hence, been pushed to a high TRL already.

4. OUTLOOK ON TECHNOLOGY DEVELOPMENT ACTIVITIES

Within and external to the LIFE initiative, many activities are ongoing to develop and increase the TRL levels of the technologies described above, or to investigate alternative approaches. We will discuss and summarize a few of these developments here, while some have been covered earlier. This summary is far from a complete review of all the ongoing activities but should give an insight into the prospering research relevant to LIFE.

4.1 Component Developments

As mentioned above, investigations for **detector** technologies alternative to the MCT or Si:As are necessary as both established technologies might not be fully applicable for the full wavelength range of LIFE, either due to their dark current characteristics or their availability in the future, respectively. KIDs are established for (sub-) millimeter and optical wavelengths but are quite unexplored in the MIR. Recent activities however showed

that the detection range of KIDs can also be extended to the MIR and dedicated investigations are planned to optimize and characterize these devices for the application of LIFE.[68] As a potential alternative, superconducting nanowire single-photon detectors are also studied in the MIR with very promising results.[69,70]

As for the **spatial filters**, a key challenge is the availability of single-mode fibers for the entire wavelength range of LIFE. One potential and efficient option could be endlessly single-mode photonic crystal waveguides that are fed by phase-induced amplitude apodization optics.[71] Furthermore, investigations for photonic devices that are suitable for MIR are ongoing (e.g., Montesinos, 2024[72]) and show promising results. If these devices become the new benchmark for MIR photonics has to be seen, but their application could reach well beyond the initial need for waveguiding and spatial filtering: The entire architecture from the achromatic phase shifter down to the cross-combiner could be built in a photonic device, similar to architectures already implemented for shorter wavelengths for ground-based applications such as kernel nulling photonic interferometers[73] or the nulling combiner for the Asgard/NOTT instrument.[74] Kernel nulling and other collector arrangements (like the 5-collector architecture) would become serious alternatives to the current baseline. In principle, these devices could even be extended to include the delay lines, the spectrometer, and eventually even the detector. However, the system efficiency for the MIR photonic platform has first to be carefully evaluated under cryogenic conditions for a broad-band source. It may be rather unlikely that these devices work achromatic and efficiently over a large wavelength range. Additionally, the reported shortfalls of near-IR photonic devices for astronomical applications[75] must first be addressed before they can be extended to MIR in a manner competitive with bulk optic architectures.

Cryogenic **deformable mirrors** are another key technology of interest. Cryogenic mirrors have been developed in the past[76–79] but these were specific developments and the devices are not commercially available. Further, the different use cases in LIFE (aberration and tip/tilt control on the one side and the potential need for an achromatic nuller) might introduce further differences in the required developments. One particular ongoing development of interest is on hysteretic deformable mirrors:[80] Their set-and-forget nature facilitates the use of time division multiplexing to address the single pixels without the need for high update frequencies to avoid pixel drift. Additionally, these devices can be stacked to adjust the total stroke, hence they might be well aligned with the different needs for LIFE.

4.2 System Level Developments

To demonstrate the feasibility of LIFE, system aspects of the mission need to be developed side by side with the TRL increases at the component level.

Most notable is the **formation flying** of multiple spacecraft with relative precision in the sub-cm-range. Fortunately, the situation today is much more advanced than at the time of the DARWIN concept studies when no civil space mission had been flow yet to employ formation flying. Several missions have been developed in the meantime. In particular, the ESA mission PROBA-3,[81] with a probable launch date still in 2024, will aim to demonstrate six-axis formation flying at the ∼1 mm and arcsec level. This provides a new benchmark for formation-flying control, autonomous operation and maneuvering without ground control. This is achieved using inter-satellite metrology systems and cold-gas micro-thrusters for fine maneuvering. When successful, this mission will undoubtedly demonstrate the reliability of the formation flying technology and that the induced complexity of metrology-based closed-loop systems can be managed within the required performance. A further step towards robust formation flying swarms consisting of more than two spacecraft was very recently made with NASA's STARLING mission, consisting of four small satellites, launched in summer of 2023. The four spacecraft fly in larger relative distances, not directly comparable to the LIFE application. Nevertheless, several experiments were conducted successfully*[82] , addressing swarm maneuver planning and execution, communications networking, relative navigation, and especially autonomous coordination between spacecraft.

However, the in-orbit **interferometric fringe tracking** in a formation-flying mission likely needs to be demonstrated. Multiple international studies are currently ongoing, with a variety of missions proposed,[83–88] with sizes stretching from cube-sats to medium-large satellites.

*https://www.nasa.gov/directorates/stmd/swarming-for-success-starling-completes-primary-mission/

Demonstrating the measurement principle in the lab is essential for any mission development. In the case of LIFE, it is required that the **nulling performance** of the beam-combiner is demonstrated while fulfilling all other key performance requirements, in particular the sensitivity to the planet signal. This requires the demonstration at cryogenic temperatures, and that the optical components are optimized for maximum system throughput. The Nulling Interferometry Cryogenic Experiment[50] (NICE) replicates a subset of the LIFE system architecture but represents the key building blocks described in the previous chapters. Therefore, the technologies required for the beam combiner of LIFE are also required for NICE. NICE is currently in its warm development phase and the development of the cryogenic components has started. NICE builds on the legacy of previous testbeds[89–91] developed during the TPF-I and Darwin area, complementing these efforts for the first time with a cryogenic demonstration.

Lastly, ground-based efforts for nulling interferometry such as Asgard/NOTT[74] will provide the framework for developing **signal processing** approaches relevant for LIFE.

4.3 Concept Study

The LIFE team is preparing for a concept study phase. Of fundamental importance is the ongoing mission requirement definition. With the system architecture presented in this paper, a first breakdown of these requirements into performance budgets will be worked out so that the required technologies can be identified. The catalog of questions to be addressed in this concept study phase is numerous and reaches over all aspects of the mission, from optical, thermal, to operational, and beyond. A first key element of the study will be the establishment of an optical design, an opto-mechanical concept and specific design studies to assess alignment and surface error accuracies. This also includes a full end-to-end wavefront propagation model to assess diffraction and wavefront error propagation that are essential to understanding the effective system throughput when using spatial filters. Chromatic effects in the optical train need to be understood very well to assess if an adaptive nuller is required or can be avoided. If such a subsystem is needed, it must be implemented in NICE as soon as possible given that the adaptive nuller has only been demonstrated in a laboratory bench once[53] and requires several transmissive elements that could introduce significant transmission losses and increase the complexity of the beam combiner. A full polarisation model will be needed in order to understand the residual errors when using the co-rotating combiner concept as presented in Section 3.3. The modulation scheme for the X-array needs to be finalized based on a trade-off study to optimize thrust and observation efficiency.

This list of open study aspects could be extended much further. The overall goal of the study phase is to reach a level of conceptual maturity where a detailed design phase can be started without the risk of identifying big conceptual omissions later on. Further, a technology development plan should clearly outline the path forward for the various investments required to enhance the feasibility of LIFE's technology.

Besides of the technical questions, a key aspect of the upcoming concept study includes also the question of how such a mission could be implemented and funded. LIFE is at this stage not yet a selected mission by any of the space agencies. While the topical theme of ESA's Voyage 2050 strategy favors a mission like LIFE, we also explore alternative approaches and elaborate on strategies to enable LIFE independently.

5. CONCLUSIONS

The Large Interferometer for Exoplanets (LIFE) represents a groundbreaking initiative in the quest to detect and characterize terrestrial exoplanets in the habitable zone. By leveraging mid-infrared nulling interferometry, LIFE aims to achieve unprecedented sensitivity and spatial resolution, enabling the detection of Earth-like planets around nearby stars and the detailed study of their atmospheres. LIFE's unique capabilities will allow for the differentiation between biological and non-biological processes, advancing our understanding of life's potential distribution in the universe.

In this paper, we presented the mission's concept and discussed the various components and technologies required to enable the ambitious space mission. LIFE will require cutting-edge technologies and precise engineering to mitigate the challenges associated with nulling interferometry at cryogenic conditions. Many technology development activities are ongoing globally that will foster LIFE. Specific system developments have been started,

such as the nulling demonstration at cryogenic conditions, and the fringe tracking in space. Continued development and refinement of the LIFE mission concept are crucial. Collaborative efforts across international scientific communities, space agencies, and the private sector will be vital in securing the necessary funding and technological support.

In conclusion, LIFE embodies the next frontier in exoplanetary exploration. By pushing the boundaries of current technology and expanding our knowledge of planetary systems, LIFE holds the promise of uncovering new worlds and, potentially, new habitations for life. The mission represents a bold step toward answering one of humanity's most profound questions: Are we alone in the universe?

ACKNOWLEDGMENTS

Part of this work has been carried out within the framework of the National Centre of Competence in Research PlanetS supported by the Swiss National Science Foundation under grant 51NF40_205606. The authors acknowledge the financial support of the SNSF.

REFERENCES

[1] L. Kreidberg, J. L. Bean, J.-M. Désert, *et al.*, "Clouds in the atmosphere of the super-Earth exoplanet GJ1214b," Nature **505**, 69–72 (Jan. 2014).

[2] T. P. Greene, T. J. Bell, E. Ducrot, *et al.*, "Thermal emission from the Earth-sized exoplanet TRAPPIST-1 b using JWST," Nature **618**, 39–42 (June 2023).

[3] S. Zieba, L. Kreidberg, E. Ducrot, *et al.*, "No thick carbon dioxide atmosphere on the rocky exoplanet TRAPPIST-1 c," Nature **620**, 746–749 (Aug. 2023).

[4] R. Hu, A. Bello-Arufe, M. Zhang, *et al.*, "A secondary atmosphere on the rocky exoplanet 55 Cancri e," *arXiv e-prints* , arXiv:2405.04744 (May 2024).

[5] F. Wunderlich, M. Scheucher, M. Godolt, *et al.*, "Distinguishing between Wet and Dry Atmospheres of TRAPPIST-1 e and f," ApJ **901**, 126 (Oct. 2020).

[6] S. P. Quanz, I. Crossfield, M. R. Meyer, *et al.*, "Direct detection of exoplanets in the 3-10 μm range with E-ELT/METIS," *International Journal of Astrobiology* **14**, 279–289 (Apr. 2015).

[7] National Academies of Sciences, Engineering, and Medicine, [*Pathways to Discovery in Astronomy and Astrophysics for the 2020s*], The National Academies Press, Washington, DC (2021).

[8] R. N. Bracewell, "Detecting nonsolar planets by spinning infrared interferometer," Nature **274**, 780–781 (Aug. 1978).

[9] C. A. Beichman, N. J. Woolf, and C. A. Lindensmith, "The Terrestrial Planet Finder (TPF) : a NASA Origins Program to search for habitable planets," tech. rep., Jet Propulsion Laboratory, California Institute of Technology, Pasadena, California (1999).

[10] S. Martin, A. Ksendzov, O. Lay, *et al.*, "TPF-Interferometer: a decade of development in exoplanet detection technology," in [*Techniques and Instrumentation for Detection of Exoplanets V*], S. Shaklan, ed., Proc. SPIE **8151**, 81510D (Oct. 2011).

[11] A. Léger, J. J. Puget, J. M. Mariotti, *et al.*, "How to evidence Primitive Life on an exo-Planet? — The DARWIN project," Space Sci. Rev. **74**, 163–169 (Oct. 1995).

[12] C. S. Cockell, T. Herbst, A. Léger, *et al.*, "Darwin—an experimental astronomy mission to search for extrasolar planets," *Experimental Astronomy* **23**, 435–461 (Mar. 2009).

[13] S. P. Quanz, M. Ottiger, E. Fontanet, *et al.*, "Large Interferometer For Exoplanets (LIFE). I. Improved exoplanet detection yield estimates for a large mid-infrared space-interferometer mission," A&A **664**, A21 (Aug. 2022).

[14] F. A. Dannert, M. Ottiger, S. P. Quanz, *et al.*, "Large Interferometer For Exoplanets (LIFE): II. Signal simulation, signal extraction, and fundamental exoplanet parameters from single-epoch observations," *Astronomy & Astrophysics* **664**, A22 (Aug. 2022).

[15] B. S. Konrad, E. Alei, S. P. Quanz, *et al.*, "Large Interferometer For Exoplanets (LIFE). III. Spectral resolution, wavelength range, and sensitivity requirements based on atmospheric retrieval analyses of an exo-Earth," A&A **664**, A23 (Aug. 2022).

[16] J. T. Hansen, M. J. Ireland, and LIFE Collaboration, "Large Interferometer For Exoplanets (LIFE). IV. Ideal kernel-nulling array architectures for a space-based mid-infrared nulling interferometer," A&A **664**, A52 (Aug. 2022).

[17] E. Alei, B. S. Konrad, D. Angerhausen, *et al.*, "Large Interferometer For Exoplanets (LIFE). V. Diagnostic potential of a mid-infrared space interferometer for studying Earth analogs," A&A **665**, A106 (Sept. 2022).

[18] J. Kammerer, S. P. Quanz, F. Dannert, *et al.*, "Large Interferometer For Exoplanets (LIFE): VI. Detecting rocky exoplanets in the habitable zones of Sun-like stars," *Astronomy & Astrophysics* **668**, A52 (Dec. 2022).

[19] J. T. Hansen, M. J. Ireland, R. Laugier, *et al.*, "Large Interferometer For Exoplanets (LIFE). VII. Practical implementation of a five-telescope kernel-nulling beam combiner with a discussion on instrumental uncertainties and redundancy benefits," A&A **670**, A57 (Feb. 2023).

[20] D. Angerhausen, M. Ottiger, F. Dannert, *et al.*, "Large Interferometer for Exoplanets: VIII. Where Is the Phosphine? Observing Exoplanetary PH_3 with a Space-Based Mid-Infrared Nulling Interferometer," *Astrobiology* **23**, 183–194 (Feb. 2023).

[21] B. S. Konrad, E. Alei, S. P. Quanz, *et al.*, "Large Interferometer For Exoplanets (LIFE). IX. Assessing the impact of clouds on atmospheric retrievals at mid-infrared wavelengths with a Venus-twin exoplanet," A&A **673**, A94 (May 2023).

[22] Ó. Carrión-González, J. Kammerer, D. Angerhausen, *et al.*, "Large Interferometer For Exoplanets (LIFE). X. Detectability of currently known exoplanets and synergies with future IR/O/UV reflected-starlight imaging missions," A&A **678**, A96 (Oct. 2023).

[23] T. Matsuo, F. Dannert, R. Laugier, *et al.*, "Large Interferometer For Exoplanets (LIFE). XI. Phase-space synthesis decomposition for planet detection and characterization," A&A **678**, A97 (Oct. 2023).

[24] D. Angerhausen, D. Pidhorodetska, M. Leung, *et al.*, "Large Interferometer For Exoplanets (LIFE). XII. The Detectability of Capstone Biosignatures in the Mid-infrared—Sniffing Exoplanetary Laughing Gas and Methylated Halogens," AJ **167**, 128 (Mar. 2024).

[25] S. P. Quanz, O. Absil, W. Benz, *et al.*, "Atmospheric characterization of terrestrial exoplanets in the mid-infrared: biosignatures, habitability, and diversity," *Experimental Astronomy* **54**, 1197–1221 (Dec. 2022).

[26] Voyage 2050 Senior Committee, [*Voyage 2050 - Final Recommendations from the Voyage 2050 Senior Committee*] (2021).

[27] P. R. Lawson, O. P. Lay, K. J. Johnston, *et al.*, "Terrestrial Planet Finder Interferometer Science Working Group Report," 212 (Mar. 2007).

[28] W. J. Borucki, "*KEPLER* Mission: Development and overview," *Reports on Progress in Physics* **79**, 036901 (Mar. 2016).

[29] L. Kaltenegger, "How to Characterize Habitable Worlds and Signs of Life," *Annual Review of Astronomy and Astrophysics* **55**, 433–485 (Aug. 2017).

[30] R. K. Kopparapu, E. Hébrard, R. Belikov, *et al.*, "Exoplanet Classification and Yield Estimates for Direct Imaging Missions," *The Astrophysical Journal* **856**, 122 (Mar. 2018).

[31] C. D. Dressing and D. Charbonneau, "The occurrence of potentially habitable planets orbiting M dwarfs estimated from the full *Kepler* dataset and an empirical measurement of the detection sensitivity," *The Astrophysical Journal* **807**, 45 (June 2015).

[32] S. Bryson, M. Kunimoto, R. K. Kopparapu, *et al.*, "The Occurrence of Rocky Habitable-zone Planets around Solar-like Stars from Kepler Data," *The Astronomical Journal* **161**, 36 (Jan. 2021).

[33] G. J. Bergsten, I. Pascucci, G. D. Mulders, *et al.*, "The Demographics of Kepler's Earths and Super-Earths into the Habitable Zone," AJ **164**, 190 (Nov. 2022).

[34] J. Kammerer and S. P. Quanz, "Simulating the exoplanet yield of a space-based mid-infrared interferometer based on *Kepler* statistics," *Astronomy & Astrophysics* **609**, A4 (Jan. 2018).

[35] B. S. Konrad, E. Alei, S. P. Quanz, *et al.*, "Large Interferometer For Exoplanets (LIFE): IX. Assessing the impact of clouds on atmospheric retrievals at mid-infrared wavelengths with a Venus-twin exoplanet," *Astronomy & Astrophysics* **673**, A94 (May 2023).

[36] J.-N. Mettler, B. S. Konrad, S. P. Quanz, *et al.*, "Earth as an Exoplanet. III. Using Empirical Thermal Emission Spectra as an Input for Atmospheric Retrieval of an Earth-twin Exoplanet," *The Astrophysical Journal* **963**, 24 (Mar. 2024).

[37] R. K. Kopparapu, R. M. Ramirez, J. SchottelKotte, *et al.*, "Habitable Zones around Main-sequence Stars: Dependence on Planetary Mass," ApJ **787**, L29 (June 2014).

[38] R. K. Kopparapu, R. Ramirez, J. F. Kasting, *et al.*, "Habitable Zones around Main-sequence Stars: New Estimates," ApJ **765**, 131 (Mar. 2013).

[39] J. R. P. Angel and N. J. Woolf, "An Imaging Nulling Interferometer to Study Extrasolar Planets," ApJ **475**, 373–379 (Jan. 1997).

[40] O. P. Lay and S. Dubovitsky, "Nulling interferometers: the importance of systematic errors and the X-array configuration," in [*New Frontiers in Stellar Interferometry*], W. A. Traub, ed., *Society of Photo-Optical Instrumentation Engineers (SPIE) Conference Series* **5491**, 874 (Oct. 2004).

[41] B. Mennesson, A. Léger, and M. Ollivier, "Direct detection and characterization of extrasolar planets: The Mariotti space interferometer," Icarus **178**, 570–588 (Nov. 2005).

[42] D. Defrère, O. Absil, R. den Hartog, *et al.*, "Nulling interferometry: impact of exozodiacal clouds on the performance of future life-finding space missions," A&A **509**, A9 (Jan. 2010).

[43] O. P. Lay, "Removing instability noise in nulling interferometers," in [*Advances in Stellar Interferometry*], J. D. Monnier, M. Schöller, and W. C. Danchi, eds., *Society of Photo-Optical Instrumentation Engineers (SPIE) Conference Series* **6268**, 62681A (June 2006).

[44] S. R. Martin, D. Scharf, R. Wirz, *et al.*, "TPF-Emma: concept study of a planet finding space interferometer," in [*Techniques and Instrumentation for Detection of Exoplanets III*], D. R. Coulter, ed., *Society of Photo-Optical Instrumentation Engineers (SPIE) Conference Series* **6693**, 669309 (Sept. 2007).

[45] N. W. Tuchow, C. C. Stark, and E. Mamajek, "HPIC: The Habitable Worlds Observatory Preliminary Input Catalog," AJ **167**, 139 (Mar. 2024).

[46] O. Guyon, B. Mennesson, E. Serabyn, *et al.*, "Optimal Beam Combiner Design for Nulling Interferometers," PASP **125**, 951 (Aug. 2013).

[47] S. Martin, D. P. Scharf, R. Wirz, *et al.*, "Design study for a planet-finding space interferometer," in [*2008 IEEE Aerospace Conference*], 1–19 (2008).

[48] E. Serabyn and M. M. Colavita, "Fully Symmetric Nulling Beam Combiners," Appl. Opt. **40**, 1668–1671 (Apr. 2001).

[49] R. O. Gappinger, R. T. Diaz, A. Ksendzov, *et al.*, "Experimental evaluation of achromatic phase shifters for mid-infrared starlight suppression," **48**(5), 868–880.

[50] M. Ranganathan, A. M. Glauser, T. Birbacher, *et al.*, "The nulling interferometer cryogenic experiment: the warm phase," *SPIE, Paper 13095-52* (2024).

[51] M. Benisty, J. P. Berger, L. Jocou, *et al.*, "An integrated optics beam combiner for the second generation VLTI instruments," A&A **498**, 601–613 (May 2009).

[52] O. Guyon, "Phase-induced amplitude apodization of telescope pupils for extrasolar terrestrial planet imaging," A&A **404**, 379–387 (June 2003).

[53] R. D. Peters, O. P. Lay, and P. R. Lawson, "Mid-Infrared Adaptive Nulling for the Detection of Earthlike Exoplanets," PASP **122**, 85 (Jan. 2010).

[54] A. L. Mieremet, J. J. Braat, H. Bokhove, *et al.*, "Achromatic phase shifting using adjustable dispersive elements," in [*Interferometry in Optical Astronomy*], P. Léna and A. Quirrenbach, eds., *Society of Photo-Optical Instrumentation Engineers (SPIE) Conference Series* **4006**, 1035–1041 (July 2000).

[55] D. Rouan, D. Pelat, M. Ygouf, *et al.*, "A new concept of achromatic phase shifter for nulling interferometry," in [*Techniques and Instrumentation for Detection of Exoplanets III*], D. R. Coulter, ed., *Society of Photo-Optical Instrumentation Engineers (SPIE) Conference Series* **6693**, 669316 (Sept. 2007).

[56] A. Gáspár, G. H. Rieke, P. Guillard, *et al.*, "The Quantum Efficiency and Diffractive Image Artifacts of Si:As IBC mid-IR Detector Arrays at 5-10 μm: Implications for the JWST/MIRI Detectors," PASP **133**, 014504 (Jan. 2021).

[57] T. L. Roellig, C. McMurtry, T. Greene, *et al.*, "Mid-infrared detector development for the Origins Space Telescope," *Journal of Astronomical Telescopes, Instruments, and Systems* **6**, 041503 (Oct. 2020).

[58] M. Dorn, C. McMurtry, J. Pipher, *et al.*, "A monolithic 2k × 2k LWIR HgCdTe detector array for passively cooled space missions," in [*High Energy, Optical, and Infrared Detectors for Astronomy VIII*], A. D. Holland and J. Beletic, eds., *Society of Photo-Optical Instrumentation Engineers (SPIE) Conference Series* **10709**, 1070907 (July 2018).

[59] T. Pichon, V. Schwartz, A. Gougeon, *et al.*, "ARIEL early engineering model H1RG IR detector: test bench description and first characterization results," in [*X-Ray, Optical, and Infrared Detectors for Astronomy X*], A. D. Holland and J. Beletic, eds., *Society of Photo-Optical Instrumentation Engineers (SPIE) Conference Series* **12191**, 121911P (Aug. 2022).

[60] J. M. Leisenring, D. Atkinson, R. Bowens, *et al.*, "Evaluating the GeoSnap 13-μm cutoff HgCdTe detector for mid-IR ground-based astronomy," *Astronomische Nachrichten* **344**, e20230103 (Oct. 2023).

[61] M. S. Cabrera, *Development of 15 μm cutoff wavelength HgCdTe detector arrays for astronomy*, PhD thesis, University of Rochester, New York (Jan. 2020).

[62] D. Atkinson, M. Meyers, R. Bowens, *et al.*, "GeoSnap: A 1024x1024 HgCdTe array covering 3-13μm," in [*Ground-Based Thermal Infrared Astronomy - Past, Present and Future*], 4 (Oct. 2020).

[63] J. Perido, J. Glenn, P. Day, *et al.*, "Extending KIDs to the Mid-IR for Future Space and Suborbital Observatories," *Journal of Low Temperature Physics* **199**, 696–703 (Feb. 2020).

[64] W. G. Ras, *Microwave Kinetic Inductance Detectors For The Mid-Infrared*, Master's thesis, University of Technology Delft, Netherlands (Nov. 2022).

[65] E. E. Wollman, V. B. Verma, A. B. Walter, *et al.*, "Recent advances in superconducting nanowire single-photon detector technology for exoplanet transit spectroscopy in the mid-infrared," *Journal of Astronomical Telescopes, Instruments, and Systems* **7**, 011004 (Jan. 2021).

[66] G. L. Pilbratt, J. R. Riedinger, T. Passvogel, *et al.*, "Herschel Space Observatory. An ESA facility for far-infrared and submillimetre astronomy," A&A **518**, L1 (July 2010).

[67] P. J. Shirron, M. O. Kimball, B. L. James, *et al.*, "Design and on-orbit operation of the soft x-ray spectrometer adiabatic demagnetization refrigerator on the Hitomi observatory," *Journal of Astronomical Telescopes, Instruments, and Systems* **4**, 021403 (Apr. 2018).

[68] W. G. Ras, K. Kouwenhoven, J. Thoen, David, *et al.*, "Experimental demonstration of photon counting with kinetic inductance detectors at mid-infrared wavelengths," *SPIE, Paper 13103-11* (2024).

[69] G. G. Taylor, A. B. Walter, B. Korzh, *et al.*, "Low-noise single-photon counting superconducting nanowire detectors at infrared wavelengths up to 29 μm," *Optica* **10**, 1672 (Dec. 2023).

[70] E. E. Wollman, G. Taylor, S. Patel, *et al.*, "Current state of mid-infrared superconducting nanowire single-photon detectors," *SPIE, Paper 13103-12* (2024).

[71] M. J. Ireland, S. Madden, and L. Rapp, "Spatial filtering for the large interferometer for exoplanets (life) mission," *SPIE, Paper 13103-12* (2024).

[72] M. Montesinos-Ballester, A. M. Glauser, L. Miller, *et al.*, "Low loss optical integrated waveguides operating over a broad mid-infrared wavelength range," *SPIE, Paper 13100-252* (2024).

[73] N. Cvetojevic, F. Martinache, P. Chingaipe, *et al.*, "3-beam self-calibrated Kernel nulling photonic interferometer," *arXiv e-prints* , arXiv:2206.04977 (June 2022).

[74] D. Defrère, G. Garreau, R. Laugier, *et al.*, "Status of the asgard/nott nulling interferometer," *SPIE, Paper 13095-14* (2024).

[75] N. Jovanovic, P. Gatkine, N. Anugu, *et al.*, "2023 Astrophotonics Roadmap: pathways to realizing multi-functional integrated astrophotonic instruments," *Journal of Physics: Photonics* **5**, 042501 (Oct. 2023).

[76] P. Rausch, S. Verpoort, and U. Wittrock, "Unimorph deformable mirror for space telescopes: design and manufacturing," *Opt. Expr.* **23**, 19469 – 19477 (2015).

[77] R. Trines, H. Janssen, S. Paalvast, *et al.*, "A cryogenic 'set-and-forget' deformable mirror," in [*Advances in Optical and Mechanical Technologies for Telescopes and Instrumentation II*], R. Navarro and J. H. Burge, eds., *Society of Photo-Optical Instrumentation Engineers (SPIE) Conference Series* **9912**, 99121B (July 2016).

[78] A. Takahashi, K. Enya, K. Haze, *et al.*, "Laboratory demonstration of a cryogenic deformable mirror for wavefront correction of space-borne infrared telescopes," Appl. Opt. **56**, 6694 (Aug. 2017).

[79] F. Zamkotsian, P. Lanzoni, R. Barette, *et al.*, "Cryo micro-deformable mirrors for next generation AO systems," in [*Adaptive Optics Systems VI*], L. M. Close, L. Schreiber, and D. Schmidt, eds., *Society of Photo-Optical Instrumentation Engineers (SPIE) Conference Series* **10703**, 1070370 (July 2018).

[80] R. Huisman, M. P. Bruijn, S. Damerio, *et al.*, "High pixel number deformable mirror concept utilizing piezoelectric hysteresis for stable shape configurations," *Journal of Astronomical Telescopes, Instruments, and Systems* **7**, 029002 (Apr. 2021).

[81] J. S. Llorente, A. Agenjo, C. Carrascosa, *et al.*, "PROBA-3: Precise formation flying demonstration mission," *Acta Astronautica* **82**, 38–46 (Jan. 2013).

[82] J. Kruger, S. S. Hwang, and S. D'Amico, "Starling Formation-Flying Optical Experiment: Initial Operations and Flight Results," *arXiv e-prints* , arXiv:2406.06748 (June 2024).

[83] J. T. Hansen and M. J. Ireland, "A linear formation-flying astronomical interferometer in low Earth orbit," *Publications of the Astronomical Society of Australia* **37**, e019 (May 2020).

[84] C. Dandumont, D. Defrère, J. Kammerer, *et al.*, "Exoplanet detection yield of a space-based Bracewell interferometer from small to medium satellites," *Journal of Astronomical Telescopes, Instruments, and Systems* **6**, 035004 (July 2020).

[85] T. Matsuo, S. Ikari, H. Kondo, *et al.*, "High spatial resolution spectral imaging method for space interferometers and its application to formation flying small satellites," *Journal of Astronomical Telescopes, Instruments, and Systems* **8**, 015001 (Jan. 2022).

[86] L. Pogorelyuk, P. Serra, S. Kacker, *et al.*, "Laser-guided space interferometer," in [*Optical and Infrared Interferometry and Imaging VIII*], A. Mérand, S. Sallum, and J. Sanchez-Bermudez, eds., *Society of Photo-Optical Instrumentation Engineers (SPIE) Conference Series* **12183**, 121831E (Aug. 2022).

[87] J. T. Hansen, S. Wade, M. J. Ireland, *et al.*, "Pyxis: a ground-based demonstrator for formation-flying optical interferometry," *Journal of Astronomical Telescopes, Instruments, and Systems* **9**, 045001 (Oct. 2023).

[88] T. Ito, "Formation-flying interferometry in geocentric orbits," A&A **682**, A38 (Feb. 2024).

[89] S. Martin, A. Booth, K. Liewer, *et al.*, "High performance testbed for four-beam infrared interferometric nulling and exoplanet detection," *Applied Optics* **51**(17), 3907 (2012).

[90] P. A. Schuller, O. Demangeon, A. Léger, *et al.*, "The NULLTIMATE test bench: achromatic phase shifters for nulling interferometry," *Optical and Infrared Interferometry II* **7734**(July), 77342E (2010).

[91] K. Ergenzinger, R. Flatscher, U. Johann, *et al.*, "EADS Astrium Nulling Interferometer Breadboard for DARWIN and GENIE," in [*5th International Conference on Space Optics*], B. Warmbein, ed., *ESA Special Publication* **554**, 223–230 (June 2004).